LAWRENCE
LIVERMORE
NATIONAL
LABORATORY

UCRL-JRNL-231546

Thermal degradation in a trimodal PDMS network by 1H Multiple Quantum NMR

J. R. Giuliani, E. Gjersing, S. Chinn, T. V. Jones, T. Wilson, C. Alviso, J. Herberg, R. S. Maxwell

June 6, 2007

Journal of Physical Chemistry

Disclaimer

Thermal degradation in a trimodal PDMS network by ^{1}H multiple quantum NMR

*Jason R. Giuliani[1], Erica L. Gjersing[2], Sarah C. Chinn[1], Ticora V. Jones[1], Thomas S. Wilson[1], Cynthia T. Alviso[1], Julie L. Herberg[1], Mark A. Pearson[1], Robert S. Maxwell[1]**

1) Lawrence Livermore National Laboratory, 7000 East Ave, Livermore, CA 94551;

2) Department of Chemical Engineering and Material Science, University of California, Davis, Davis, CA 95616;

RECEIVED DATE

Running title: Thermal degradation of trimodal silicone networks by ^{1}H MQ-NMR

*CORRESPONDING AUTHOR FOOTNOTE. Ph: (925) 423-4991; fax: (925) 423-3720; email: Maxwell7@llnl.gov

UCRL-JRNL-231546

ABSTRACT. Thermal degradation of a filled, crosslinked siloxane material synthesized from PDMS chains of three different average molecular weights and with two different crosslinking species has been studied by ^{1}H Multiple Quantum (MQ) NMR methods. Multiple domains of polymer chains were detected by MQ NMR exhibiting Residual Dipolar Coupling ($<\Omega_d>$) values of 200 Hz and 600 Hz, corresponding to chains with high average molecular weight between crosslinks and chains with low average molecular weight between crosslinks or near the multifunctional crosslinking sites. Characterization of the $<\Omega_d>$ values and changes in $<\Omega_d>$ distributions present in the material were studied as a function of time at 250 °C and indicates significant time dependent degradation. For the domains with low $<\Omega_d>$, a broadening in the distribution was observed with aging time. For the domain with high $<\Omega_d>$, increases in both the mean $<\Omega_d>$ and the width in $<\Omega_d>$ were observed with increasing aging time. Isothermal Thermal Gravimetric Analysis (TGA) reveals a 3% decrease in weight over 20 hours of aging at 250 °C. Degraded samples also were analyzed by traditional solid state ^{1}H NMR techniques and offgassing products were identified by Solid Phase MicroExtraction followed by Gas Chromatography-Mass Spectrometry (SPME GC-MS). The results, which will be discussed here, suggest that thermal degradation proceeds by complex competition between oxidative chain scissioning and post-curing crosslinking that both contribute to embrittlement.

KEYWORDS. degradation, siloxanes, bi-modal networks, multiple quantum NMR

UCRL-JRNL-231546

INTRODUCTION

Silica filled polydimethylsiloxane composite systems can be synthesized with a broad range of structural variables including the degree and type of crosslinking, the molecular weight between crosslinks, the number of elastically ineffective chains (loops, dangling chain ends, sol-fraction) as well as filler content and surface properties.[1] Currently, high performance silicone elastomer formulations with bi- or tri-modal network structures and/or highly functional crosslinking junctions are of particular interest for commercial manufacturing. Such networks show enhanced mechanical properties even in un-filled composites and are stable in the presence of environmental, radiative, and chemical degradation.[2-4] Given the stability of these polymers, service lifetimes are often nonlinear and sensitive experimental methods are necessary to monitor structural and motional changes that occur over time. Of particular interest here are the thermal degradation pathways that have traditionally been monitored using mass spectrometry, Fourier transform infra-red spectrometry, or gel permeation chromatography.[5-7] However, these methods only monitor volatile or semi-volatile degradation products or pathways involving soluble degradation fractions of the polymer network.

Chemiluminescence has gained appreciable attention for identifying and quantifying the transient initial chemical species created by oxidative chain scission reactions.[5,8-10] Nuclear magnetic resonance (NMR) has also been used to characterize chemical speciation changes occurring in both soluble and insoluble fractions, however with limited sensitivity. For example, Alam and coworkers[11-13] have shown that aging silicone samples in an ^{17}O isotopically enriched atmosphere, followed by ^{17}O NMR on swollen samples, can provide sensitive and selective detection of rare reaction products due to incorporation of the ^{17}O label in the network and in soluble reaction products. However, these methods only yield insight into chemical speciation changes and do not provide direct insight into molecular weight (MW) distribution changes and

UCRL-JRNL-231546

the resultant changes to the polymer dynamics that determine the physical properties of the material.

In contrast, static ^{1}H NMR spectroscopy has shown an increasing ability to characterize elastomer network structure and heterogeneities as well as dynamic processes in a non-destructive fashion.[2,11-27] Several methods exist to extract residual anisotropic interactions which relate directly to macroscopic polymer properties.[28] Recent developments in ^{1}H Multiple Quantum (MQ) NMR methods allow for the measurement of absolute residual dipolar couplings ($<\Omega_d>$) and segmental/cooperative dynamics throughout elastomeric materials without interference from magnetic susceptibility and field gradients which have been observed in relaxation measurements.[19,22,23,26,27] In elastomeric materials, $<\Omega_d>$ results from topological constraints interfering with fast reorientations on the NMR timescale that otherwise would be expected to average homonuclear dipolar couplings to zero. Such $<\Omega_d>$ values and their distributions are proportional to the degree of chain coupling-junctions and directly related to the dynamic order parameter S_b of the polymer backbone.[24,29] Furthermore, since the engineering properties (e.g. tensile, shear, creep moduli, etc.) are largely dependent on network topology and filler-particle interactions, MQ methods offer the potential for model-free insight into the structure-property relationships and the origins of degradation in material performance.

Given the sensitivity of MQ NMR methods in monitoring network and morphological changes, such methods are ideal for the investigation of thermal degradation of complex silicone composites. The materials under investigation here are constructed from PDMS chains of three average chain lengths and crosslinked with Tetra-n-propoxysilane [TPS] (functionality, ϕ=4) and PolyMethylHydroSilane [PMHS] (ϕ=60) using standard condensation reactions.[1,14] We are interested in degradation pathways occurring during the thermal 'induction period'[5] where temperatures remain below critical decomposition thresholds. Since thermal degradation, oxidation, and hydrolysis are typical high temperature responses of organic materials in general,

similar pathways would be expected for the current material. Specifically, Zeldin et al.[30] found network rearrangements in PDMS samples at 250 ºC which proceeded from a hydrolysis pathway and others have found low molecular weight cyclic volatiles resulting from hydroxyl-terminated materials.[6,31-34] In addition, Lai et al.[35] have found crosslinker hydrolysis to lead to degradation under mild aging conditions. Many of these degradation pathways can lead to build up of low molecular weight fragments, thus reducing molecular weights in polymer networks and increasing the quantity of dangling chain ends which can be directly detected using various NMR methods.

EXPERIMENTAL

Materials: The silicone network studied here was produced using standard Sn-octanoate catalyzed, endlinking silicone chemistry.[1,14] The network was constructed from a combination of hydroxyl-endlinked PDMS with three different average molecular weights [High Molecular Weight (HMW): M_n = 13,600 , M_w = 58,300; Medium Molecular Weight (MMW): M_n = 11,700, M_w = 27,400; Low Molecular Weight (LMW): M_n = 1,530 , M_w = 1,850] and two different crosslinking units [Tetra-n-propoxysilane (TPS): FW = 264 g/mol, ϕ = 4] and PolyMethylHydroSilane (PMHS) [M_n = 3,700, M_w = 8,200, ϕ = 60]. Here the functionality of the crosslinking sites, ϕ, is the number of available sites per molecule for crosslinking. In addition, DiPhenylMethylSilane (DPMS: FW = 214 g/mol, ϕ = 1) was added as a blowing agent and low temperature modifier. All the above materials were obtained from NuSil [Carpenteria, CA]. The base resin was made by mixing all three hydroxyl-endlinked PDMS units [46.5 wt% HMW, 15.5 wt% MMW, and 12.0 wt% LMW], diatomaceous earth filler [15 wt%], TPS [2 wt%], DPMS [5 wt%], and PMHS [4 wt%] with a mechanical mixer until homogeneous. Network foams were created by adding 5% by weight Sn-octanoate catalyst to the base resin at room temperature and mixing for approximately 15 s. The catalyzed resin was then immediately

poured into the mold, closed, and allowed to cure for a minimum of 15 min. The reaction of the silanol sites of the PDMS chains with the silane sites on the PMHS produces H_2 which forms the pore structure as the network cures. The foamed network was then allowed to air cure at room temperature for a minimum of 16 h followed by post-curing at 240°C for 3 to 3.5 h. The chemical species and an illustration of the resulting network are shown in **Figure 1**. Average crosslink density and mechanical properties were previously reported by Gjersing et al.[14] as sample SX462.

Thermal Gravimetric Analysis: Thermal gravimetric analysis (TGA) was performed on SX462 using a Mettler TGA model SDTA851e. The 21.462 mg specimen was made up of several thin pieces, which were cut from a single thin sheet, and loosely stacked within an open 70 μL alumina crucible. The protection gas was UltraZero air administered at a rate of 20 ml/min. Isothermal TGA experiments were run for 20 hours at 250°C. The instrument required approximately 5 minutes to reach the desired temperature and then weight loss was measured as a function of time. Traditional TGA experiments were performed within a temperature range of 25°C to 800°C with a ramp rate of 10.0°C per minute. A blank analysis was also performed to reduce possible error associate with the analysis, including the buoyancy effect.

Solid Phase Micro Extraction (SPME) Materials: Carboxen/PDMS (85 μm) SPME fibers were purchased from Supelco. SPME headspace vials (20 mL), crimp caps and septa (20 mm, teflon/blue silicone, level 4) were purchased from MicroLiter Analytical Supplies. Three samples, weighing approximately 20-30 mg each, were placed in 20 mL SPME headspace vials. One set (one control and one sample) was left at room temperature. The other two sets were aged by placing them in a 100˚C oven and a 250˚C oven, respectively. Analysis was conducted following 30 minutes of aging, eight hours (additional seven and a half hours) of aging, and 16 hours (additional eight hours) of aging.

UCRL-JRNL-231546

SPME Characterization: Headspace SPME analyses for a given time period and temperature were performed on a blank control vial and SX462 sample. The samples were analyzed by SPME GC/MS using an automated system under the following conditions: 85 μm Carboxen/PDMS SPME fiber, conditioned between samples for five minutes at 260˚C; headspace sampled at 50˚C for 20 minutes and injected into the GC for one minute at 250˚C. The Agilent 6890 GC was set for splitless injection and purged at 0.5 minutes using a J & W Scientific DB-624 column (30 m, 0.25 mm ID, 1.4 μm film) with a 1.0 mL/min constant flow of helium. The 20 minute run had the following temperature profile: 40˚C/1.05 min., 23.41˚C/min. to 260˚C, and held 6.81 min. An Agilent 5973 mass spectrometer scanned the mass range from 35-450 at a rate of 1.81 scans/s with no filament delay. Outgassing products were identified by comparison of their mass spectra to the NIST 02 mass spectral library.

NMR Methods: All spin-echo and MQ experiments were performed on a Bruker Avance 400 spectrometer with a ^{1}H frequency of 400.013 MHz. Samples with dimensions (3 mm x 3 mm x 2 mm) were centered within the coil volume of a Bruker TBI (HCX) 5 mm probe with 90^{o} pulse lengths τ_p = 4.50 μs. Traditional ^{1}H Hahn-spin echo experiments were performed as previously described[29,36,37] with recycle delay times of 6 s. Multiple quantum NMR experiments were performed as described by Saalwächter et al.[19,26] using the generic pulse sequence to excite even-quantum coherences shown in **Figure 2**. Double quantum (DQ) coherences, containing all excited 2n+2 quantum orders, were selected using a four-step reconversion phase cycle with 90^{o} steps while phase inverting the receiver on alternate scans. In addition, the read pulse and receiver were synchronously incremented in a CYCLOPS fashion to yield a sixteen-step phase cycle. Reference MQ coherences, containing all excited 4n quantum orders, were selected using the DQ selection phase cycle without receiver alternation. All experiments were preformed by n_c incrementing the DQ mixing time ($\tau_{DQ}=a(\psi)n_c t_c$) with cycle times (t_c) of 180 μs and the finite

nature of the rf pulses compensated for using the scaling factor $a(\psi)=1-12*(\tau_p/t_c)$ rigorously derived elsewhere.[26,36]

NMR Analysis: Echo intensity curves were fit to a bi-exponential decay representing two separate relaxation processes

$$E.I.(\tau) = X_{short} e^{-\frac{2\tau}{T_{2short}}} + X_{long} e^{-\frac{2\tau}{T_{2long}}} \quad \{1\}$$

where X_i are the mole fractions of chains in each domain, τ the delay between the 90° and 180° pulses, and T_{2i} are the transverse relaxation time of each domain. The domains with the short T_2 are typically assigned to the polymer chains associated with the crosslinked network while the domains with the long T_2 are assigned to the chains associated with the uncrosslinked, sol-fraction.[26] The spin-echo decay cures obtained in this study did not show any sign of the pseudo-solid decays observed in other PDMS networks, indicating that the motional processes are rapid compared to other crosslinked elastomers.[17]

The DQ build-up curves were normalized as previously described by Saalwächter and coworkers[26] by dividing each point in the DQ build-up curve by the total MQ signal

$$I_{nDQ}(\tau_{DQ}) = \frac{S_{DQ}(\tau_{DQ})}{S_{MQ}(\tau_{DQ})} \quad \{2\}$$

where $S_{MQ}(\tau_{DQ})$ results from both the DQ and reference build-up curves

$$S_{MQ}(\tau_{DQ}) = S_{DQ}(\tau_{DQ}) + S_{ref}(\tau_{DQ}) - S_{ref}^{*}(\tau_{DQ}) \quad \{3\}$$

and $S_{ref}^{*}(\tau_{DQ})=A*\exp(-\tau_{DQ}/T_{2A})$ represents the liquid-like contribution to the total MQ signal decay typically attributed to sol content of polymer networks. Finally, the normalized DQ build-up curves did not show any temperature dependence over the range of 300-340 K indicating that the separation of timescales assumption was valid in these polymers. The temperature independence of the normalized MQ growth curve indicates that the measured residual dipolar

couplings are due solely to fast averaging of the anisotropic motional processes and not to any additional interfering motions such that the RDCs directly reflect the polymer chain structure.[26]

The dipolar couplings contributing to the normalized DQ build-up curve can be extracted within the second-moment approximation as an inverted Gaussian with the following form

$$I_{nDQ}(\langle\Omega_d\rangle;\tau_{DQ}) = 0.5*(1-e^{-\frac{2}{5}\langle\Omega_d\rangle^2\tau_{DQ}^2}) \quad \{4\}$$

where it is assumed that $<\Omega_d>$ follows static Gaussian statistics. If distributions of coupling frequencies exist within a sample, Saalwächter et al.[26] has shown that the analytical form of the integral over **Equation 4** results in the following closed form equation

$$I_{nDQ}(\langle\Omega_d\rangle,\sigma_d;\tau_{DQ}) = 0.5*\left(1-\frac{e^{-\frac{\frac{2}{5}\langle\Omega_d\rangle^2\tau_{DQ}^2}{1+2\frac{2}{5}\sigma_d^2\tau_{DQ}^2}}}{\sqrt{1+2\frac{2}{5}\sigma_d^2\tau_{DQ}^2}}\right) \quad \{5\}$$

where $<\Omega_d>$ and σ_d are the average dipolar coupling and distribution width respectively. Alternatively, **Equation 4** can be used as a kernel function to regularize the distribution interval of coupling frequencies using the fast Tikhonov regulation FTIKREG.[26,38]

The relationship between the residual dipolar coupling and polymer structural variables has been described using the scale-invariant model and extensively described elsewhere.[22,29,39-41] These studies have correlated the residual dipolar couplings to the dynamic order parameter, S_b, and to the number of statistical segments, N, between constraints:

$$S_b = \frac{1}{P_2(\cos\alpha)}\frac{\langle\Omega_d\rangle}{\langle\Omega_d\rangle_{static}} = \frac{3r^2}{5N} \quad \{6\}$$

where $<\Omega_d>_{static}$ is the dipolar coupling in the absence of motion (but pre-averaged by the fast motion of the methyl group) and equal to 8900 Hz, $<P_2(\cos\alpha)>$ is the time-averaged second order Legendre polynomial of the angle between the dipolar vector and the chain axis (i.e. the angle between the chain axis and the Si-C vector, taken here to be 90°), and r is the vector

describing the deviation of the end-to-end vector, **R**, from that of the unperturbed melt, $\mathbf{R}_o$: $r=\mathbf{R}/\mathbf{R}_o$.[26]

The normalized DQ build-up curve shown in **Figure 3A** deviates from the inverted Gaussian model given in **Equation 4**. In this case it reasonable to assume the sample has a bimodal or phase separated network structure described by a summation of growth curves

$$I_{DQ}(\langle\Omega_d\rangle;\tau_{DQ}) = \sum X(\Omega_i) * 0.5 * (1 - e^{-\frac{2}{5}\langle\Omega_d\rangle_i^2 \tau_{DQ}^2}) \qquad \{7\}$$

where $X(\Omega_i)$ is the relative mole fraction of spins. The coupling frequencies and fractions resulting from a *least-squares* minimization of the DQ build-up curve over the normalized intensity region of 0.12-0.45 performed in MatLab (Mathworks) using a Gauss-Newton nonlinear optimization algorithm are presented in **Table 1**. Similarly, a bimodal representation of the Gaussian distribution model described in **Equation 5**

$$I_{DQ}(\langle\Omega_d\rangle,\sigma_d;\tau_{DQ}) = \sum X(\Omega_i) * I_{nDQ}(\langle\Omega_d\rangle_i,\sigma_{d,i}) \qquad \{8\}$$

was used to extract coupling frequencies, standard deviations and mole fractions from normalized DQ build-up curves (**Table 1**) where each distribution width was constrained to the range of 0-0.5($<\Omega_d>_i$). A representative data curve is shown in **Figure 3A** displaying fits to **Equation 7** and **8** in dashed and solid lines respectively. Sample data curves for the pristine sample and the sample aged for 20h are shown in Figure 3B.

The fast Tikhonov regulation FTIKREG was used to regularize the distribution interval of coupling frequencies for each sample over the normalized intensity region of 0.12-0.45 using **Equation 4** as the kernel function.[26,38] The stability of the regularization results were highly dependent on FTIKREG setup parameters such as estimated data errors and method used to calculate the regularization parameter. In the present case the program calculated the relative error scaling factor and the regularization parameter was calculated using the self-consistent (SC)-method where the second derivative of the identity vanishing smoothly at the upper or

UCRL-JRNL-231546

lower boundaries was used for operator L ($Lf = f''$).[38] The probability distribution obtained from regularization was fit to a sum of Gaussian functions in MatLab (Mathworks) using a Gauss-Newton nonlinear optimization algorithm and extracted coupling frequencies and standard deviations are presented in **Table 2**.

^{1}H Magic Angle Spinning (MAS) NMR experiments were performed at 500.08 MHz using a Bruker DRX spectrometer and a Bruker 4 mm High-Resolution MAS probe. Recycle delays of 10 seconds and spinning speeds of 11 kHz were used for these experiments. Chemical shifts were referenced to an external TMS standard and were assigned as follows: PDMS methyl resonances at 0.1 ppm, DPMS methyl resonances at 0.6 ppm, alkyl resonances from residual catalyst and TPS at 0.94, 1.3, and 1.6 ppm, ether methylene protons at 3.7 ppm, residual silane at 4.8 ppm and phenyl protons at 7.3 and 7.5 ppm. Integration of the silane resonance indicated that after the initial post curing a residual 4±2 % of the original silane species remains unreacted. ^{1}H MAS experiments of the 20 hr degraded sample also contained ~ 4±2 % residual silane species – roughly 96% conversion, based on what we would expect from composition.

RESULTS AND DISCUSSION

Thermal aging of the current trimodal network occurred at a temperature (250^{o}C), slightly above the cure temperature of 240^{o}C. Isothermal TGA data, shown in **Figure 4A**, indicates minimal weight loss (~3%) after 16 h of aging at 250^{o}C. Analysis of TGA data shown in **Figure 4B** indicates the first signs of decomposition at 250^{o}C with full decomposition onset measured at 389^{o}C which is consistent with other reported PDMS values.[42] Because of the lack of significant degradation at 250°C, this aging temperature was chosen to accelerate low temperature aging pathways without invoking high temperature degradation mechanisms such as random chain cleavage and complete polymer unzipping.[30]

SPME GC/MS analysis was used to identify outgassing signatures of volatile and semi-volatile compounds as a function of time at 250°C. Total ion chromatographs for samples aged at 250°C for eight and sixteen hours are shown in **Figure 5**. Signatures with intensities above 5% of the maximum peak, with the exception of those that were present in the blank, were identified and are listed in **Table 3**. The largest signatures are attributed to benzene (5.76 minutes) and various cyclosiloxanes (tri-, tetra-, and pentasiloxanes at 6.76, 8.03, and 9.16 minutes, respectively). The presence of cyclosiloxanes is consistent with previous analysis of offgassing species from thermally degraded silicones that underwent oxidative chain scissioning and hydrolysis reactions.[6,31-34] The presence of benzene is attributed to a degradation product of the DPMS blowing agent. The other significant signature at 9.51 minutes was assigned to 2-ethylhexanoic acid, a hydrolysis product of the tin octanoate catalyst,[43,44] which indicates the presences of residual catalyst and the potential for post-cure reactions. Smaller signatures seen in **Figure 5** and assigned in **Table 3** are likely degradation products of the TPS crosslinking agent and tin octanoate catalyst. These signatures were assigned to various alcohols (traditional hydrolysis products), aldehydes, carboxylic acids and ketones (traditional oxidation products), though these products could also result from condensation or other post-cure reactions. Interestingly, the same signatures were observed in the sample aged for eight hours and that aged for sixteen hours, though the sixteen-hour sample displayed a larger concentration of the species with the exception of the 2-ethylhexanoic acid signature. This would suggest that the completion of the post-cure process at shorter times and a dominance of traditional degradation via hydrolysis/oxidation at longer times at elevated temperature.

NMR spin echo relaxation times (**Table 1**), were found to be independent of aging time within experimental error. This data suggests that the ensemble averaged relaxation times unique to both fast relaxing crosslinked components ($T_2 \sim 1.5$ ms) and slow relaxing sol-fraction ($T_2 \sim 12$ ms) remain constant during the degradation process. However, a decrease in the fractional

occupancy of fast relaxing contributions to the spin-echo decay curve was observed and is shown in **Figure 6**. The increase in the highly mobile fraction of polymer chains is in agreement with the SPME results and is likely due to an increase in both the amount of dangling chain ends and sol fraction brought about by oxidative chain scission and backbiting reactions. Such reactions are well documented in the literature.[5-10]

The complex nature of the normalized DQ build-up curves, as demonstrated in **Figure 3A**, reflect a distribution of residual dipolar couplings around at least two means, as described, for example, by a superposition of inverted Gaussians described in **Equation 7**. The rapid rise of the build-up curve from τ_{DQ}=0.00-0.36 ms and the drastic deviation from either a simple discrete two site model (**Equation 7**) or a superposition of two Gaussian populations (**Equation 8**) has been generally absent from most PDMS resins studied to date, but has been observed by Saalwächter for a small subset of samples.[26] The deviation at short build-up times indicates strong coupling interactions of ^{1}H nuclei. The interactions could be due to chains very close to highly functional crosslinking sites, chains associated with the filler, or highly entangled domains of the polymer network. The complexity of the growth curve in this region and the limited number of data points obtainable (the lowest increment of τ_{DQ} achievable in our setup was 0.17 ms) limit the ability to quantify either the residual dipolar coupling or to accurately estimate the population of this site as the sample aged. As a result, the present study focuses on low frequency coupling modes ($\langle\Omega_d\rangle$ < 1500 Hz) which dominate the growth curve for τ_{DQ}>0.36 ms.

The extracted $\langle\Omega_d\rangle$ and $X(\Omega_1)$ values from fits of the normalized DQ build-up curves to **Equation 7** and **8** are shown in **Table 1** and trends in the coupling values are depicted in **Figure 7A**. The chains characterized by low frequency ($\langle\Omega_d\rangle$ ~ 200 Hz) are assigned to the $Si(CH_3)_2O_{2/2}$- monomers in the low crosslink density chains. The chains characterized by residual dipolar couplings near 600 Hz are assigned to $Si(CH_3)_2O_{2/2}$- monomers in the high

crosslink density chains and monomers near the highly functional PMHS crosslinking sites. The populations of these two sites agrees well with what would be expected from the formulation details, as described in Gjersing, et al.[14] Using an inverted Gaussian shown in **Equation 7** to fit the normalized DQ build-up curves results in $<\Omega_d>$ and $X(\Omega_1)$ values inversely proportional to aging time at 250°C, suggesting the domination of chain scissioning degradation. Similar analysis using two site fitting functions with Gaussian distribution of coupling frequencies, as shown in **Equation 8**, resulted in $<\Omega_d>$ values that were observed to increase slightly with aging time as shown in **Figure 7B.** In this figure, the vertical bars superimposed on the $<\Omega_{d,i}>$ values represent the distribution width $\sigma_{d,i}$ extracted from the normalized DQ data at each time point. The increase in the low frequency $\sigma_{d,i}$ with aging time indicates that the low frequency coupling mode broadens to encompass a larger distribution of coupling frequency during the aging process, due to combined effects of chain scission and crosslinking reactions.

The distribution of $<\Omega_d>$ values resulting from fast Tikhonov regularization of each sample is shown in **Figure 8** and the extracted coupling values and standard deviations are presented in **Table 1** and shown graphically in **Figure 7C**. The pristine sample is characterized by three distributions of residual dipolar couplings. The two lower residual dipolar coupling distributions are assigned as the distributions obtained using the discrete two site model or the two-Gaussian model, discussed above. The source of the very high residual dipolar coupling population ($<\Omega_d>$ ~ 1000 Hz) is due to the regularization routine attempting to fit the initial high intensity for $\tau_{DQ} < 0.36$, as mentioned earlier. Again, due to the limited data, the distributions obtained in this regime are subject to large regularization errors. Given the inherent errors, we draw no quantitative conclusions on this domain and it is ignored in the discussion below.

The coupling distributions (**Figure 8**) present several visual trends in the temperature dependence of the measured dipolar coupling. As highlighted in the above results, the changes in low frequency peak width upon increased thermal aging are clearly depicted. The changes in

peak breadth are again illustrated in **Figure 7C** and compared with similar results obtained from fitting the normalized DQ data to **Equation 8**. The higher frequency coupling modes also were observed to significantly increase in mean frequency and broaden as thermal aging progressed.

Although the distribution functions calculated using FTIKREG are semiquantitative in nature,[22] the relative distribution changes observed for this family of samples and with equivalent FTIKREG processing parameters can be compared to generate insight into relevant degradation mechanisms occurring during thermal aging and to reflect the relative physical and chemical changes occurring within the polymer network. Detailed discussion of the relevance of the distribution widths can be found in Saalwächter et al.[26] Further, the trend of increased distribution width for $<\Omega_d>$ from the regularization analysis is similar to the trend from fitting the growth curve to a two site Gaussian distribution model. This gradual frequency broadening indicates that the polymer networks far from crosslinking sites are undergoing a complex combination of post-curing crosslinking and oxidative, thermally activated, chain scissioning reactions. The FTIKREG results agree well with those obtained using **Equation 7** (inverted Gaussian function).

As discussed above, the data shown in **Figure 7** and **Tables 1 and 2** was obtained from analyzing the MQ growth curves by three different processes: discrete two site model (**Equation 7**), two narrow Gaussian distributions (**Equation 8**), and Tikhonov regularization using **Equation 4** as a kernel. The three methods yield roughly similar trends, yet different quantitative results for the time dependence of the fractional populations in the two domains and the mean residual dipolar couplings. Despite the results of the discrete two site fit, it can clearly be seen in **Figure 3B** that there is an increase in the early time slope and a decrease in the late time slope of the growth curve for the sample aged for 20 hr. This shape in the growth curve is entirely consistent with an increase in the $<\Omega_d>$ for the high crosslink density site and an increase in the distribution in the $<\Omega_d>$ for the low crosslink density distribution. Such an increase in the

UCRL-JRNL-231546

distribution in the low crosslink density chains is consistent in trend, if not in explicit value, for both the overlapping Gaussian distribution and the FTIKREG results. This trend indicates that the chains in the low crosslink density domains are undergoing further crosslinking reactions as well as chain scissioning reactions. The changes in the high crosslink density chains are more complex, given the conflicting results from the Gaussian distribution and the FTIKREG regularization process. Since the discrete two site fit cannot effectively fit the growth curve at early excitation times, it does not yield sufficient insight into the changes occurring in this domain. Additionally, the FTIKREG regularization is likely hampered by the limited amount of points in the early excitation time region, as discussed above. Due to the noted limitations in the various fitting methods, we put more confidence in the overlapping Gaussian deconvolution in **Figure 7B**, which suggests that the high crosslink density domain increases in average $<\Omega_d>$ slightly while narrowing slightly in distribution with time.

The MQ NMR results presented here, particularly the two analysis methods that reflect distributions in the RDC, are consistent with the SPME analysis of the volatile and semivolatile degradation species and the observation that the material is more brittle after aging. As discussed above, the SPME data agrees well with previous analysis of offgassing species from thermally degraded silicones and suggests oxidative chain scissioning and hydrolysis reactions. The SPME results show large contributions from cyclic siloxanes which are a known degradation product of siloxane elastomers, and they are likely formed due to thermally activated depolymerization reactions along the siloxane chain, as suggested by Hall et al.[6], and originally proposed by Osthoff et al.[45] Such low temperature scission processes are known to occur by hydrolysis mechanisms[46] under atmospheric conditions at weak/strained Si-O linkages. In the present material, the tetra-crosslinked TPS nodes most likely represent the weakest points within the polymer network. These reactions would be expected to increase the sol-fraction and number of dangling chain ends in the polymer network as observed from the spin-echo analysis. The

decrease in fast relaxing network components observed in the spin-echo experiments suggests that thermal aging decreases network population adjacent to crosslinking sites in a nonrandom, oxidative scission type fashion as previously observed.[30]

The MQ NMR results also indicate a mechanism by which the chain dynamics are reduced, presumably through crosslinking reactions. Crosslinking during thermal aging at similar temperatures was previously observed for unfilled PDMS samples by Grassie et al.[31] Continued post-curing reactions of the residual silane species present from unreacted sites on the PMHS crosslinking moiety would lead to increased crosslink density for all chains. ^{1}H MAS NMR analysis of the pristine and aged samples showed no difference as a function of aging time within experimental error. However, given the very small amount of residual silane protons detected (less than 0.05 % of the proton inventory) and the expected loss of protons from other degradation processes (~3% from TGA), the lack of quantifiable difference in silane concentration would be expected. The limited amount of propyl alcohols, aldehydes or acids observed by SPME GC/MS analysis indicates that post-curing of the silanes is also accompanied by mild crosslinking seen due to branching reactions within long chain PDMS network components. Given the large offgassing of benzene observed in the SPME results, this is likely due to reaction of free radical terminated chain ends with PDMS chains nearby to increase the branching in the network.

CONCLUSIONS

The use of MQ NMR experiments to study the thermal aging process of complex PDMS networks has been shown. Using several complementary methods of analyzing DQ build-up curves indicates that degradation in these complex PDMS networks occurs by a combination of oxidative chain scission reactions and crosslinking reactions, likely involving post-curing at the unreacted silane sites and random formation of branching due to crosslinking at chain ends,

following offgassing of benzene from the endcapping DPMS species. All NMR results are supported by SPME GC/MS and TGA data. The general use of MQ NMR to obtain semiquantitative insight into changes in distributions of chain structure could provide a sensitive complementary technique to other methods of analysis for degradation of complex, crosslinked PDMS networks.

ACKNOWLEDGMENTS

This work was performed under the auspices of the U.S. Department of Energy by the Lawrence Livermore National Laboratory under contract # W-7405-ENG-48. The authors would like to thank Eric Eastwood, Dan Bowen, and Jim Schneider for providing the network material studied here. This work was supported by the Laboratory Directed Research and Development program with tracking code 05-SI-006.

REFERENCES

(1) Brook, M. A. *Silicon in Organic, Organometallic and Polymer Chemistry*; John Wiley & Sons: New York, 2000.
(2) Maxwell, R. S.; Chinn, S. C.; Solyom, D.; Cohenour, R. *Macromolecules* **2005**, *38*, 7026-7032.
(3) Chang, C. L.; Don, T. M.; Lee, H. S. J.; Sha, Y. O. *Polymer Degradation and Stability* **2004**, *85*, 769-777.
(4) Mitra, S.; Ghanbari-Siahkali, A.; Almdal, K. *Polymer Degradation and Stability* **2006**, *91*, 2520-2526.
(5) Celina, M.; Trujillo, A. B.; Gillen, K. T.; Minier, L. M. *Polymer Degradation and Stability* **2006**, *91*, 2365-2374.
(6) Hall, A. D.; Patel, M. *Polymer Degradation and Stability* **2006**, *91*, 2532-2539.
(7) Zhou, W. J.; Yang, H.; Guo, X. Z.; Lu, J. J. *Polymer Degradation and Stability* **2006**, *91*, 1471-1475.
(8) Zlatevich, L. *Luminescence techniques in solid state polymer research*; Marcel Dekker: New York, 1989.
(9) Celina, M.; Clough, R. L.; Jones, G. D. *Polymer Degradation and Stability* **2006**, *91*, 1036-1044.
(10) Ashby, G. E. *Journal of Polymer Science* **1961**, *50*, 99.
(11) Alam, T. M. *Radiation Physics and Chemistry* **2001**, *62*, 145-152.
(12) Alam, T. M.; Celina, M.; Assink, R. A.; Clough, R. L.; Gillen, K. T.; Wheeler, D. R. *Macromolecules* **2000**, *33*, 1181-1190.
(13) Alam, T. M.; Celina, M.; Assink, R. A.; Clough, R. L.; Gillen, K. T. *Radiation Physics and Chemistry* **2001**, *60*, 121-127.

(14) Gjersing, E.; Chinn, S.; Maxwell, R. S.; Giuliani, J. R.; Herberg, J.; Eastwood, E.; Bowen, D.; Stephens, T. *Macromolecules, submitted* **2007**.
(15) Maxwell, R.; Chinn, S.; Balazs, B.; Gee, R. *Abstracts of Papers of the American Chemical Society* **2003**, *225*, U629-U629.
(16) Maus, A.; Hertlein, C.; Saalwachter, K. *Macromolecular Chemistry and Physics* **2006**, *207*, 1150-1158.
(17) Maxwell, R. S.; Balazs, B. *Journal of Chemical Physics* **2002**, *116*, 10492-10502.
(18) Saalwächter, K. *Journal of the American Chemical Society* **2003**, *125*, 14684-14685.
(19) Saalwächter, K. *Journal of Chemical Physics* **2004**, *120*, 454-464.
(20) Saalwächter, K. *Macromolecules* **2005**, *38*, 1508-1512.
(21) Saalwächter, K.; Gottlieb, M.; Liu, R. G.; Oppermann, W. *Macromolecules* **2007**, *40*, 1555-1561.
(22) Saalwächter, K.; Herrero, B.; Lopez-Manchado, M. A. *Macromolecules* **2005**, *38*, 9650-9660.
(23) Saalwächter, K.; Herrero, B.; Lopez-Manchado, M. A. *Macromolecules* **2005**, *38*, 4040-4042.
(24) Saalwächter, K.; Heuer, A. *Macromolecules* **2006**, *39*, 3291-3303.
(25) Saalwächter, K.; Kleinschmidt, F.; Sommer, J. U. *Macromolecules* **2004**, *37*, 8556-8568.
(26) Saalwächter, K.; Ziegler, P.; Spyckerelle, O.; Haidar, B.; Vidal, A.; Sommer, J. U. *Journal of Chemical Physics* **2003**, *119*, 3468-3482.
(27) Saalwächter, K. *Progress in NMR Spectroscopy* **2007**, *51*, 1-35.
(28) Litvinov, V. M.; De, P. P. *Spectroscopy of Rubbers and Rubbery Materials*; Rapra Technology Ltd.: Shawbury, 2002.
(29) Cohen Addad, J. P. *Progress in NMR Spectroscopy* **1993**, *25*, 1-316.
(30) Zeldin, M.; Qian, B. R.; Choi, S. J. *Journal of Polymer Science Part a-Polymer Chemistry* **1983**, *21*, 1361-1369.
(31) Grassie, N.; Macfarlane, I. G. *European Polymer Journal* **1978**, *14*, 875-884.
(32) Grassie, N.; Macfarlane, I. G.; Francey, K. F. *European Polymer Journal* **1979**, *15*, 415-422.
(33) Kucera, M.; Lanikova, J. *Journal of Polymer Science* **1961**, *54*, 375-&.
(34) Kucera, M.; Lanikova, J. *Journal of Polymer Science* **1962**, *59*, 79-&.
(35) Lai, S. K.; Batra, A.; Cohen, C. *Polymer* **2005**, *46*, 4204-4211.
(36) Mehring, M. *Principles of High Resolution NMR in Solids*; Springer-Verlag: Berlin, 1983.
(37) Bovey, F. A. *NMR of polymers*; Academic: San Diego, 1996.
(38) Weese, J. *Computer Physics Communications* **1992**, *69*, 99-111.
(39) Callaghan, P. T.; Samulski, E. T. *Macromolecules* **2000**, *33*, 3795-3802.
(40) Grinberg, F.; Kimmich, R.; Moller, M.; Molenberg, A. *Journal of Chemical Physics* **1996**, *105*, 9657-9665.
(41) Schneider, M.; Gasper, L.; Demco, D. E.; Blumich, B. *Journal of Chemical Physics* **1999**, *111*, 402-415.
(42) Deshpande, G.; Rezac, M. E. *Polymer Degradation and Stability* **2002**, *76*, 17-24.
(43) Labouriau, A.; Taylor, D.; Stephens, T.; Pasternak, M. *Polymer Degradation and Stability* **2006**, *91*, 1896-1902.
(44) Labouriau, A.; Cox, J. D.; Schoonover, J. R.; Patterson, B. M.; Havrilla, G. J.; Stephens, T.; Taylor, D. *Polymer Degradation and Stability* **2007**, *92*, 414-424.
(45) Osthoff, R. C.; Bueche, A. M.; Grubb, W. T. *Journal of the American Chemical Society* **1954**, *76*, 4659-4663.

(46) Thomas, D. K. *Polymer* **1966**, *7*, 99.

UCRL-JRNL-231546

TABLES

Table 1. Results from bimodal fits to spin echo decay curves and normalized DQ build-up curves.

	Spin Echo		Inverted Gaussian			Inverted Gaussian with Narrow Frequency Distribution				
Aging Time (h at 250°C)	$X_1(T_{2,1})$	$T_{2,1}$ (ms)	$X(\Omega_1)$	Ω_1(Hz)	Ω_2(Hz)	$X(\Omega_1)$	Ω_1(Hz)	σ_1(Hz)	Ω_2(Hz)	σ_2(Hz)
0	0.962	1.46	0.632	167	827	0.509	161	4	630	318
4	0.964	1.41	0.615	167	823	0.496	158	19	639	314
8	0.957	1.46	0.595	161	818	0.489	157	33	649	309
12	0.934	1.45	0.594	155	801	0.511	156	44	665	317
16	0.934	1.49	0.585	151	799	0.514	149	42	676	282
20	0.923	1.47	0.579	115	789	0.513	153	46	678	292

Table 2. Results from fast Tikhonov regularization of normalized DQ build-up curves.

Aging Time (h at 250°C)	$X(\Omega_1)$	Ω_1(Hz)	σ_1(Hz)	Ω_2(Hz)	σ_2(Hz)	Ω_3(Hz)	σ_3(Hz)
0	0.753	166	42	473	55	1053	85
4	0.776	173	63	527	72	1384	144
8	0.785	179	79	621	91	-	-
12	0.802	176	94	666	116	-	-
16	0.734	192	119	1114	219	-	-
20	0.738	195	121	1136	225	-	-

UCRL-JRNL-231546

Table 3. Identification of species in total ion chromatograph from SPME analysis for sample aged at 250°C (shown in **Figure 5**). All samples over an intensity of 5% with the exception of those found on the blank SPME fiber and vial were identified.

Retention time (minutes)	Species
4.96	1-Propanol
5.18	Methylvinylketone
5.26	2-Butanone
5.51	Acetic acid
5.76	Benzene
6.09	2-Pentanone
6.16	Pentanal
6.37	Propanoic acid
6.66	1-Octanone
6.76	Hexamethyl cyclotrisiloxane
6.99	2-Hexanone
7.11	Butanoic acid
7.58	2-n-Butylacrolein
7.64	3-Hexanone
7.75	3-Heptanone
7.82	2-Heptanone
7.87	Hexanoic acid
8.03	Octamethyl cyclotetrasiloxane
8.57	2-Octanone
8.65	Octanal
8.77	2-Ethylmethylester hexanoic acid
8.86	Furanone
8.95	Phenol
9.16	Decamethyl cyclopentasiloxane
9.51	2-Ethylhexanoic acid
10.35	4,4'-[methylethylidene]bis-2,6-dimethylphenol

UCRL-JRNL-231546

FIGURE CAPTIONS

Figure 1. Composition of the starting materials used to formulate the networks studied here.

Figure 2. ^{1}H MQ Pulse Sequence used in this study. Solid lines represent 90° pulses and dashed lines represent 180° pulses. The number of pulse trains, n_c, was incremented to generate growth curves. Phasing of the detection pulse was alternated to generate the reference curve.

Figure 3. (A) Initial points of normalized double quantum build-up curve for the pristine material showing fits to functions derived from the static second-moment approximation (dashed) and Gaussian distributions (solid). (B) DQ build-up curves for pristine (solid line) and 20 h aged (dashed line) samples.

Figure 4. (A) Isothermal Thermal Gravimetric Analysis showing fractional polymer weight loss with increasing aging time at 250^{o}C; (B) Thermal Gravimetric Analysis of SX462 silicone sample.

Figure 5. Total ion chromatograph from SPME headspace analysis of SX462 aged at 250°C for 8 hours, and 16 hours.

Figure 6. Results of bimodal fits to spin-echo decay curves after various thermal aging times at 250^{o}C. Trends in fractional occupancy of fast relaxing contributions spin-echo decay curve with increasing aging time at 250^{o}C.

Figure 7. Results from fits of normalized double quantum build-up curves to functions derived from the (A) static second-moment approximation, (B) Gaussian distributions, and (C) fast Tikhonov regularization after various thermal aging times at 250^{o}C. Open circles represent low frequency coupling modes and closed circles represent high frequency coupling modes. Error bars represent the distribution widths for the Gaussian and FTIKREG distributions.

Figure 8. Dipolar coupling (Ω) distributions obtained from fast Tikhonov regularization after various thermal aging times at 250^{o}C.

UCRL-JRNL-231546

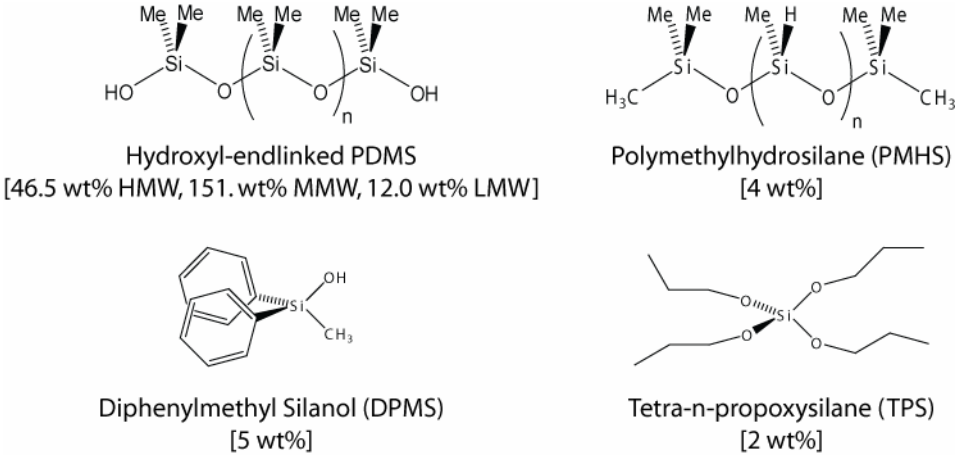

Figure 1. Giuliani et al.

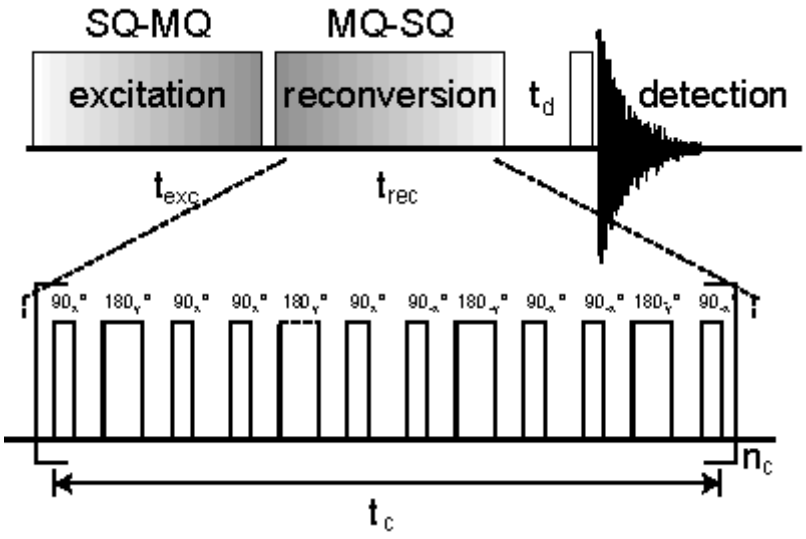

Figure 2. Giuliani et al.

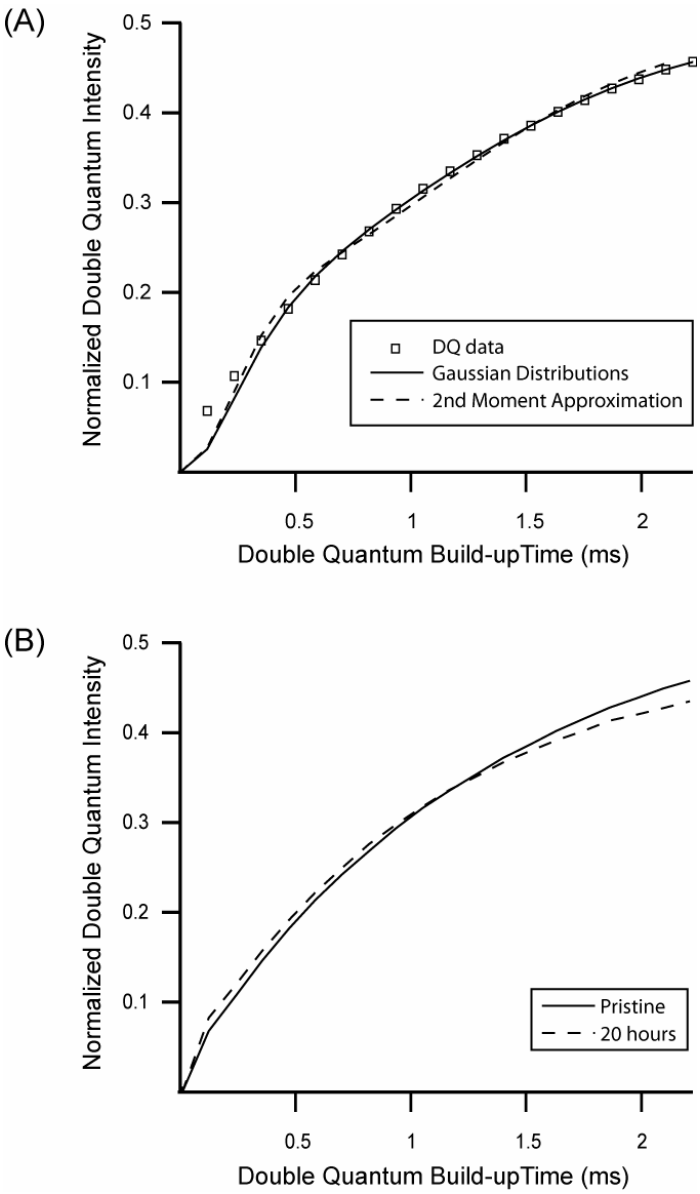

Figure 3. Giuliani et al.

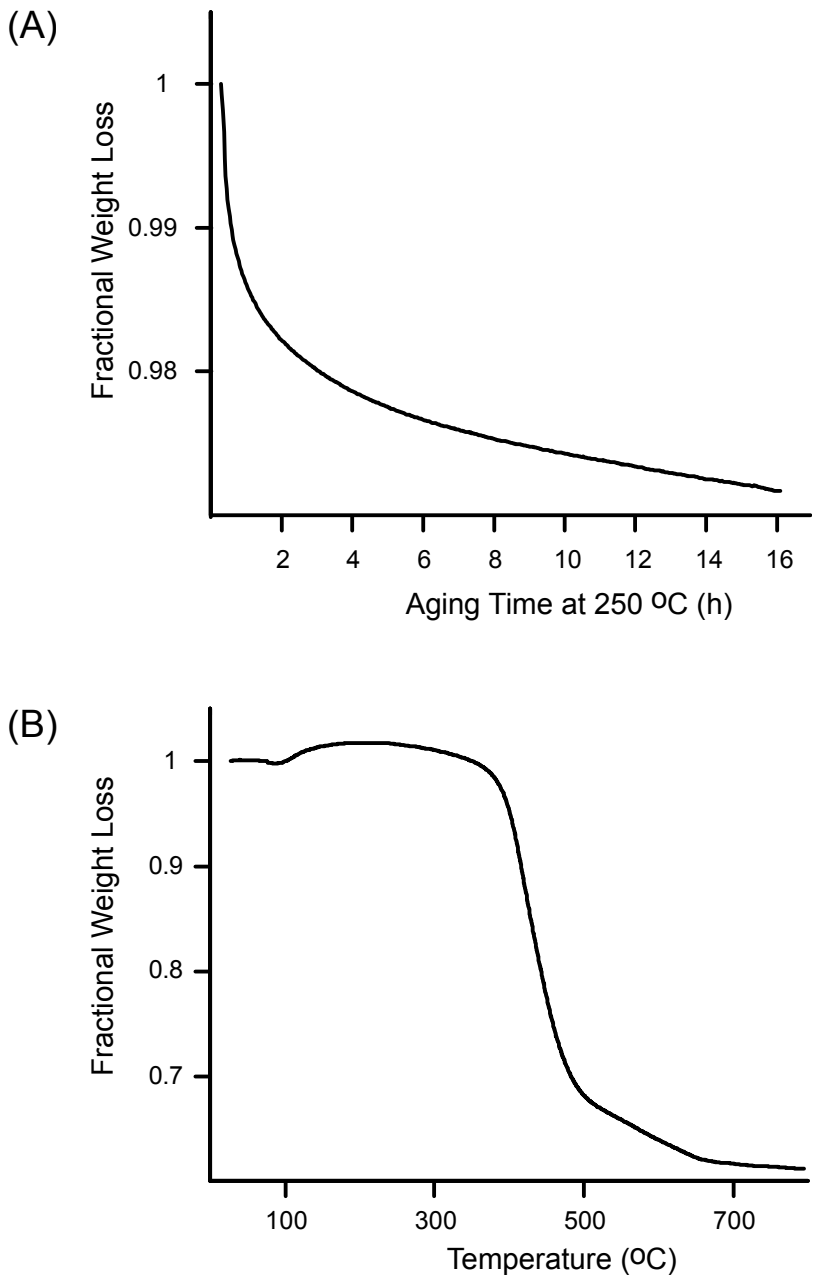

Figure 4. Giuliani et al.

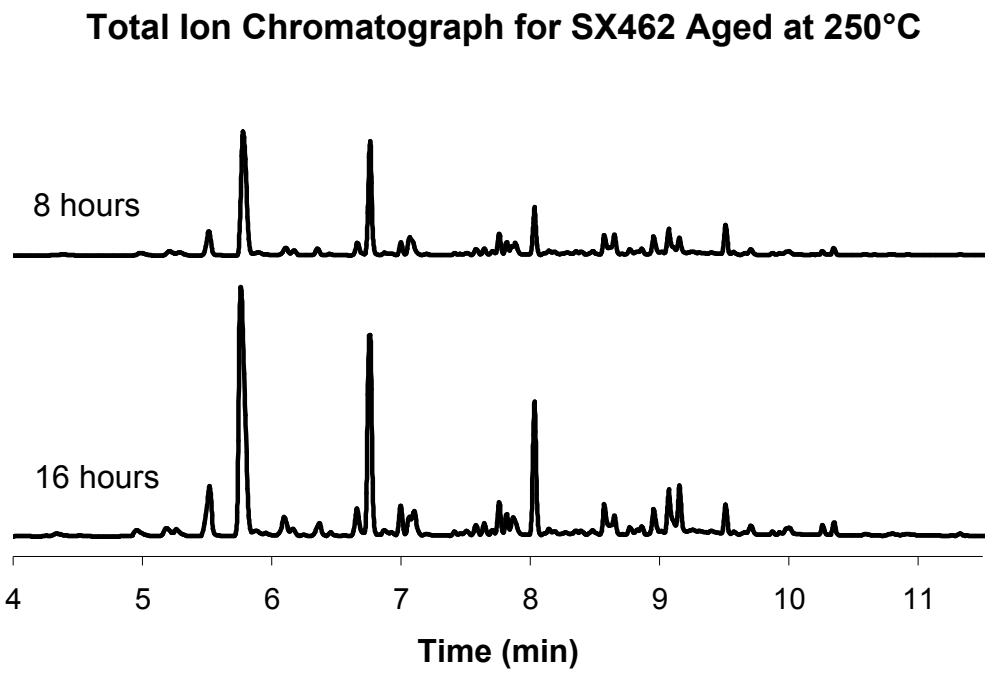

Figure 5. Giuliani et al.

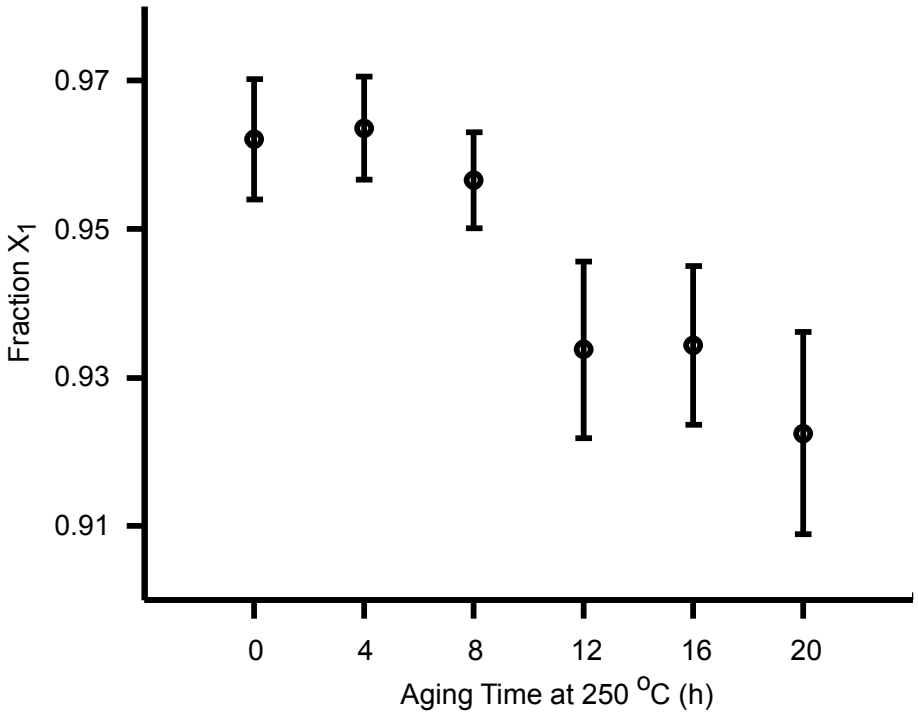

Figure 6. Giuliani et al.

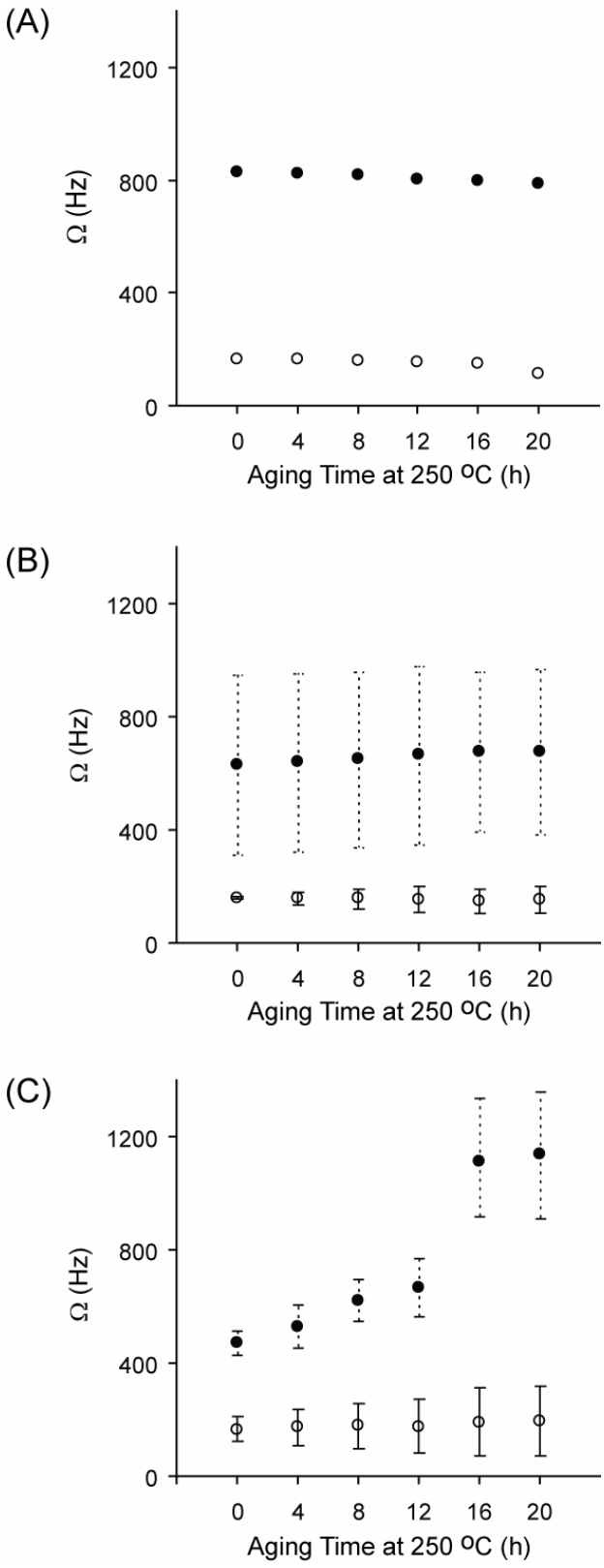

Figure 7. Giuliani et al.

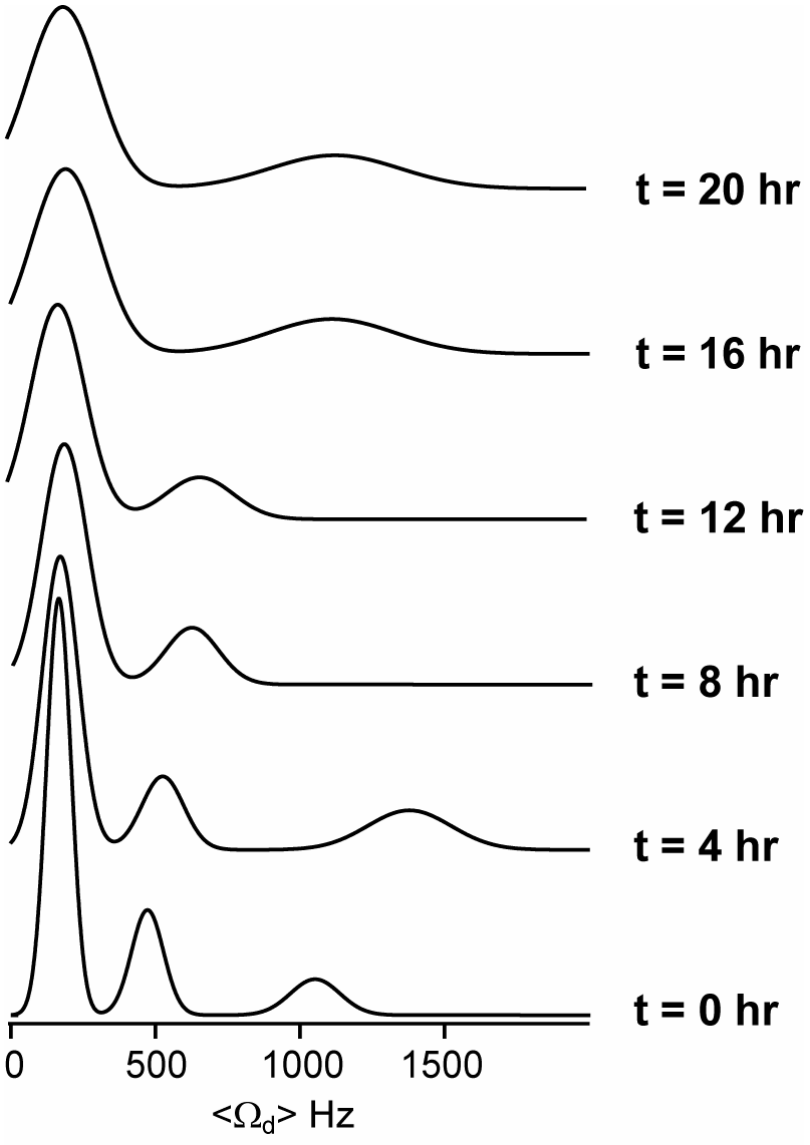

Figure 8. Giuliani et al.